Tréhu, A.M., Bohrmann, G., Torres, M.E., and Colwell, F.S. (Eds.)
Proceedings of the Ocean Drilling Program, Scientific Results Volume 204

2. Seismic Sequence Stratigraphy and Tectonic Evolution of Southern Hydrate Ridge[1]

Johanna Chevallier,[2,3] Anne M. Tréhu,[2] Nathan L. Bangs,[4] Joel E. Johnson,[2,5] and H. Jack Meyer[6]

ABSTRACT

This paper presents a seismic sequence and structural analysis of a high-resolution three-dimensional seismic reflection survey that was acquired in June 2000 in preparation for Ocean Drilling Program (ODP) Leg 204. The seismic data were correlated with coring and logging results from nine sites drilled in 2002 during Leg 204. The stratigraphic and structural evolution of this complex accretionary ridge through time, as inferred from seismic-stratigraphic units and depositional sequences imaged by the seismic data, is presented as a series of interpreted seismic cross sections and horizon time or isopach maps across southern Hydrate Ridge. Our reconstruction starts at ~1.2 Ma with a shift of the frontal thrust from seaward to landward vergent and thrusting of abyssal plain sediments over the older deformed and accreted units that form the core of Hydrate Ridge. From ~1.0 to 0.3 Ma, a series of overlapping slope basins with shifting depocenters was deposited as the main locus of uplift shifted northeastward. This enigmatic landward migration of uplift may be related to topography on the subducted plate, which is now deeply buried beneath the upper slope and shelf. The main locus of uplift shifted west to its present position at ~0.3 Ma, probably in response to a change to a seaward-vergent frontal thrust and related sediment underplating and duplexing. This structural and stratigraphic history has influenced the distribution of gas hydrate and free gas by causing variable age and permeability of sediments beneath and within the gas hydrate stability zone, preferential path-

[1] Chevallier, J., Tréhu, A.M., Bangs, N.L., Johnson, J.E., and Meyer, H.J., 2006. Seismic sequence stratigraphy and tectonic evolution of southern Hydrate Ridge. *In* Tréhu, A.M., Bohrmann, G., Torres, M.E., and Colwell, F.S. (Eds.), *Proc. ODP, Sci. Results,* 204: College Station, TX (Ocean Drilling Program), 1–29. doi:10.2973/odp.proc.sr.204.121.2006
[2] COAS, Oregon State University, Ocean Administration Building 104, Corvallis OR 97331, USA. Correspondence author: **trehu@coas.oregonstate.edu**
[3] Present address: Wintershall AG, Friedrich-Ebert-Strasse 160, D-34119 Kassel, Germany.
[4] Institute for Geophysics, University of Texas at Austin, Austin TX, USA.
[5] Present address: Department of Earth Sciences, University of New Hampshire, 56 College Road, James Hall 121, Durham NH 03824, USA.
[6] Northwest Natural Gas, 220 Northwest Second Avenue, Portland OR 97209, USA.

Initial receipt: 26 April 2005
Acceptance: 25 May 2006
Web publication: 2 November 2006
Ms 204SR-121

ways for fluid migration, and varying amounts of decompression and gas dissolution.

INTRODUCTION

Accretion of sediments to the North American plate in response to oblique subduction of the Juan de Fuca plate beneath North America at a rate of ~4 cm/yr has formed a large accretionary prism composed of Pliocene and Pleistocene strata deformed into north–south-striking folded thrust slices (e.g., Seely et al., 1974; Snavely, 1987; MacKay et al., 1992; Goldfinger et al., 1996; McNeill et al., 2000). Hydrate Ridge, a 10-km-wide, 15-km-long ridge located 17.5 km east of the Cascadia deformation front ~100 km offshore Newport, Oregon, is one of these thrust slices (Fig. F1). Deep-penetration seismic-reflection data indicate that it is composed of several juxtaposed thrust folds and faults and has a steep western flank that has repeatedly been subjected to slope instability (Tréhu et al., 1999, **Tréhu et al.,** this volume; **Johnson et al.,** this volume).

Gas hydrates are present in the shallow sediments beneath Hydrate Ridge, as indicated by a widespread bottom-simulating reflection (BSR) (e.g., Tréhu et al., 1999) and by observations of gas hydrates, methane bubbles, and hydrate-related authigenic carbonates near the northern and southern summits (e.g., Bohrmann et al., 1998; Tréhu et al., 1999; Suess et al., 2001; Torres et al., 2002; Tryon et al., 2002; Johnson et al., 2003). Recent studies have focused on determining the amount of gas hydrate present (Milkov et al., 2003; Tréhu et al. 2004a), the dynamics of gas hydrate formation near the summit (Milkov et al., 2004; Torres et al., 2004a), the plumbing system feeding the summit deposits (Tréhu et al., 2004b), and the response of the gas hydrates to changes in sea level and water temperature (Bangs et al., 2005). Logging data and core recovery from Ocean Drilling Program (ODP) Leg 204 show that gas hydrate deposits within the gas hydrate stability zone (GHSZ) range from massive to patchy to absent, with hydrate generally filling, on average, <5% of the pore space but comprising as much as 25% of the sediment volume in a focused deposit at the southern summit (Tréhu et al., 2004a).

The primary objective of this paper is to reconstruct the stratigraphic and structural development of southern Hydrate Ridge (SHR) through a detailed analysis of three-dimensional (3-D) seismic data that were collected as a site survey for Leg 204. The lithologic characteristics of seismic facies and the timing of events are constrained using sedimentological and biostratigraphic data from ODP Leg 204 (Tréhu, Bohrmann, Rack, Torres, et al., 2003). The influence of structure and lithology on the free gas and gas hydrate distribution is also discussed.

DATA

3-D Seismic Data

Multichannel 3-D seismic data were collected during summer 2000 on the *Thomas Thompson* (Tréhu and Bangs, 2001). The survey covers a 4 km × 9 km region that includes the southern summit of Hydrate Ridge and an adjacent slope basin to its east (Fig. F1C). The ship was navigated by Global Positioning System (GPS) provided by Racal (in-

F1. Location of Hydrate Ridge, p. 17.

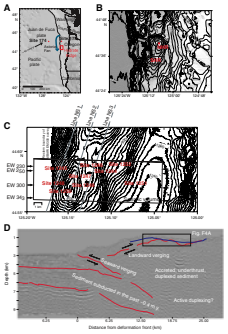

cluding differential GPS [dGPS] corrections from a weighted average of four Racal base stations). These raw fixes were recorded at 1 Hz. They were smoothed to remove the rolling and pitching of the ship for derivation of the location and the velocity of the ship at each update and were corrected to compensate for the offset of the source from the GPS antenna. The streamer's geometry was determined by four bird compasses positioned at 150-m intervals. These records were used to reposition each single receiver channel. There was no tail buoy for independent determination of the location of the end of the streamer. The depths and the wing angles of the birds were monitored by the watch-stander using a graphical display. Shots were fired at 15-m intervals based on the smoothed velocity estimate from the dGPS fixes. The source was two generator-injector (GI) guns, each set at 45/45 in^3, towed at a depth of 2.5 m, and fired simultaneously. They proved to be a good broadband source, producing usable energy from 10 to 240 Hz. The signal was recorded on a portable, 600-m-long, 48-channel streamer, which was towed at a depth of 2.5 m.

The bridge used the Nav99 program written by Mark Weidenspahn (University of Texas Institute for Geophysics) to steer the source location down the selected line. Nav99 also provided a minimum radius turn path between lines, which were always shot heading east in the northern half of the grid and heading west in the southern half. Recorded trace length was 6 s. The 3-D survey grid consisted of 81, 11-km-long east-west sections that were shot 50 m apart in a racetrack pattern. During the cruise, 3-D fold was monitored based on streamer reconstruction to identify locations where additional data were needed in order to obtain adequate fold in each bin. This resulted in reshooting 18 lines because of variable degrees of streamer feathering or navigational problems resulting from strong currents. Onboard the *Thomas Thompson*, the raw SEGD field data were copied from 3480 tapes to SEGY disk files using Sioseis. The SEGY disk files were then converted to Paradigm Geophysical's FOCUS internal format. Seven bad channels were deleted at this stage. Data were processed at sea as two-dimensional (2-D) lines for quality control and a first look at the data. Source navigation and streamer location data for the 3-D grid were converted to universal transverse Mercator (UTM) coordinates and written in UKOOA90 format. These navigation data were converted into FOCUS format 3-D navigation traces and binned using the FOCUS 3-D QC/binning package. Fold maps were generated and optimized for 50 m $\times$ 25 m and 25 m $\times$ 12.5 m bin sizes. In both cases, the optimum grid azimuth was 348.5°.

On land, data were sorted into 12.5 m $\times$ 25 m bins for the 3-D processing and renumbered from 200 to 360 to accommodate interpolated lines. A velocity analysis was done for every 10th line and every 100th common midpoint (CMP). A high-pass filter with a ramp from 15 to 25 Hz was applied to the traces to remove noise resulting from choppy seas and a large swell. The data were then corrected for normal moveout (NMO), the inner trace was muted (to attenuate the seafloor multiple), and the data were stacked. A 3-D poststack Kirchhoff migration using stacking velocities was applied. This yields the 3-D volume, which is 4 km wide $\times$ 9 km long and contains a frequency range of 20 to 180 Hz with a dominant frequency of 125 Hz, resulting in a nominal resolution of 3 m (1/4 wavelength). The continuity of north-south and time slices through the data volume, however, is degraded by static effects due to tidal changes in water depth, swell, and changes in the towing depth of the streamer and/or GI guns.

2-D Seismic Profiles

Six regional 2-D lines were recorded on the same multichannel streamer (Tréhu and Bangs, 2001). The tracks of the three north-south lines used during this study are shown on Figure F1C. The shot interval for these lines was 37.5 m, and data were sorted into 12.5-m bins, resulting in 16- to 24-fold data. A high-pass filter was applied with a ramp from 25 to 35 Hz. The data were corrected for NMO, stretch mute was done with a 35% maximum stretch, and the data were stacked assuming a constant velocity of 1500 m/s. A velocity of 1500 m/s was also used for frequency-wave-number migration of the data.

ODP Leg 204

Nine sites were drilled within the boundaries of the 3-D survey during ODP Leg 204 (Fig. F1C). The maximum coring depth ranged from 90 to 540 meters below seafloor (mbsf). Sediment classification was recorded based on visual observation and core description, smear slide analysis, and correlation with physical property data (Shipboard Scientific Party, 2003a). Mudstones and siltstones of turbidite origin, debris-flow deposits, and intervening hemipelagic clays dominate the lithologies observed in the Leg 204 cores. Classification of sediments into lithologic units was based on sometimes subtle changes in major and minor lithologies, changes in biogenic content, changes in magnetic susceptibility, and changes in the frequency and thickness of turbidite layers. Absolute ages of strata were determined based on the bioevents distinguished in the cores and presented in the Leg 204 *Initial Reports* volume (Tréhu, Bohrmann, Rack, Torres, et al., 2003). The biostratigraphic zones were inferred from the first and last occurrences of diatoms and calcareous nannofossils. Biostratigraphic ages and lithologic units determined by the Leg 204 shipboard sedimentologists are summarized in Figure F2. Although this lithologic and biostratigraphic information was used to aid in the interpretation of the seismic data, seismic units (also shown in Fig. F2) were determined independently from the lithologic units based on seismic stratigraphic packages, as outlined in **"Use of Sequence Stratigraphy in a Tectonically Active Environment."** The boundaries between lithologic and seismic units generally coincide.

F2. Lithologic units, p. 18.

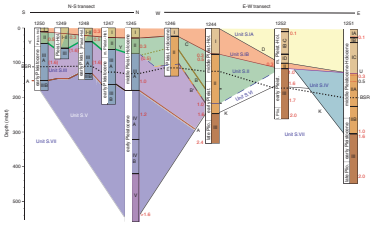

USE OF SEQUENCE STRATIGRAPHY IN A TECTONICALLY ACTIVE ENVIRONMENT

Sequence stratigraphic analysis is based on the identification of depositional sequences, which are stratigraphic units composed of a relatively conformable succession of genetically related strata bounded by two major unconformities (Mitchum, 1977). This method is usually used to reconstruct the effects of sea level rise and fall on the history of deposition on continental margins. Seismic stratigraphic analysis of SHR strata differs from traditional sequence stratigraphy in that the stratal succession was not significantly influenced by sea level changes. SHR is located on the continental slope at 800 m depth (Fig. F1), and the sediments composing the core of the ridge originated from accretion of abyssal plain sediment originally deposited at ~2900 m depth. Deposition of the overlying slope basin sediments was controlled by the formation and evolution of the accretionary wedge fold-thrust belt

system. In spite of the difference between the processes controlling changes in sediment deposition patterns, similar types of angular unconformities can be distinguished based on the geometry of the strata and their termination (Fig. F3). The unconformities bound sets of relatively concordant strata. Each of these sets is interpreted to represent one depositional sequence. Each seismic unit is subdivided into a few depositional sequences. Characteristics of the sequences are controlled by syn- and postdepositional tectonic activity.

Seismic sequence analysis of the depositional sequences mapped at SHR was used to reconstruct the sedimentary and tectonic events that deformed the sediments in the SHR fold and thrust system and the concomitant active basins and to derive a relative time-correlation of these events. The method included evaluating the relationship between the synsedimentary thrust and fold systems responsible for the formation of the ridge and the migration of the intervening slope basins. The primary tectonic processes observed on SHR are thrust-related folding of the strata and migration of the thrust system. These processes control the location and growth of sediment depocenters and result in tilting of the strata on the limbs of folds and/or along the flanks of subsiding depocenters.

F3. Nomenclature for growth strata, p. 19.

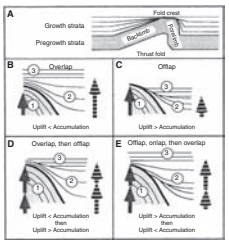

INTERPRETATION OF SEISMIC UNITS AND STRUCTURES

In this section we describe the characteristics of the seismic units and relate them to the lithologic units described by Leg 204 shipboard sedimentologists (Shipboard Scientific Party, 2003a). We illustrate our conclusions by showing several interpreted transects through the seismic volume (Fig. F4A–F4B, F4C–F4D), selected details of the seismic data, and maps of key stratigraphic horizons or fault surfaces. Further details are discussed in Chevallier (2004).

F4. East-west slices through the 3-D seismic volume, p. 21.

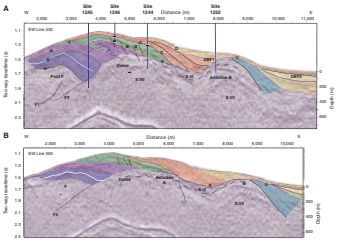

Although velocity constraints are available from ocean-bottom seismometers deployed during the 3-D seismic survey (Arsenault et al., 2001), from sonic logs during Leg 204 (Lee and Collett, this volume; Guerin et al., this volume), and from vertical seismic profiles (VSPs) during Leg 204 (Tréhu et al., this volume), velocities within the strata imaged by the 3-D survey and discussed in this paper are generally <1800 m/s and the interval velocity above the BSR is <1600 m/s. Because of the difficulty of interpolating the velocity field to define velocity at all data points in the 3-D data set and degradation of data quality because of variable stretch due to local velocity variations (some of which are real and some of which may be artifacts), data are presented here with a vertical axis of two-way traveltime. Because the average velocities are uniformly low, the effect on stratigraphic and structural patterns is small. A constant velocity of 1600 m/s in the subsurface is adequate to estimate horizon depths and isopach thicknesses throughout the 3-D data volume.

Seismic Units

The seismic units fall into two different groups: sediments deposited on the abyssal plain and transferred to the accretionary complex and sediment deposited in slope basins overlying the accreted sediments.

Abyssal Plain Sediments of the Astoria Fan

Unit S.VII represents deep-sea fan sediments older than 1.6 Ma (late Pliocene) and Unit S.V represents younger deep-sea fan sediments of age 1.6–1.1 Ma (Fig. F2). Unit S.VII is characterized by a high degree of lithification and microfracturing (Shipboard Scientific Party, 2003b, 2003d, 2003e), consistent with its long history of burial and deformation. Internal structures in these units are poorly preserved. Glauconite-rich layers near the top of this sequence indicate extended periods of exposure on the seafloor (Shipboard Scientific Party, 2003b, 2003c, 2003d, 2003e).

Unit S.V is composed of nannofossil-rich silty claystone interspersed with thick turbidites containing wood fragments that was deposited rapidly (~70 cm/k.y.) (Shipboard Scientific Party, 2003c) in the trench as part of the Astoria Fan. The top of this seismic unit is defined by Horizon A, a 2- to 4-m-thick, coarse-grained, volcanic-ash-rich turbidite layer that appears as an bright reflection in the 3-D data. Drilling revealed that Horizon A contains abundant free gas and plays a critical role in transporting methane to feed methane vents and formation of massive gas hydrate at the summit (Tréhu et al., 2004b).

Slope Basin Sediments

At Sites 1244 and 1252, Unit S.VII is overlain by sediments with an age that overlaps Unit S.V but have characteristics that are similar to Unit S.VII. We call this Unit S.VI. Seismically, it is difficult to distinguish Unit S.VI from Unit S.VII. Sediments recovered from this zone are relatively lithified and fractured and contain abundant glauconite similar to Unit S.VII, reflecting exposure on the seafloor and a very low sedimentation rate. Combining biostratigraphic data with the structural reconstruction presented in **"Tectonic History of Southern Hydrate Ridge,"** p. 9, we conclude that these sediments were deposited on the lower slope of the overriding plate near a seaward-vergent frontal thrust fault.

Slope-basin sediments younger than ~1.0 Ma overlie Units S.VII–S.V (Figs. F2, F4). These sediments (Units S.IV to S.IA) filled a migrating series of depocenters created by temporal and spatial variations in the locus of uplift. They are composed mostly of turbidites interlayered with hemipelagic silty clays. The main distinction between the lithologic units is related to the frequency and thickness of turbidites. Units S.III and S.II in the western part of the survey were deposited in the lower slope basin formed by Fold F (Fig. F4). Distinct reflections B and B′ (Fig. F4A), found at the base of and within Unit S.II, result from coarse-grained gas-rich horizons similar to Horizon A. Horizons B and B′ host gas hydrate or free gas, depending on whether they were sampled within or beneath the GHSZ (Tréhu et al., 2004a; **Guerin et al.**, this volume). Units S.III and S.II are thickest in the saddle between the northern and southern summits of Hydrate Ridge (Fig. F5).

In the eastern part of the survey region, Unit S.IV is a locally thick deposit that developed contemporaneous with Units S.III and S.II in association with Anticline B (see **"The Dome and Anticlines A and B,"** p. 7). It is separated by an unconformity (U in Figs. F2, F4) from Units S.IB and S.IA, which fill a regional basin that has been deepening to the south with time as SHR has been uplifted (Fig. F4). The lithologic unit corresponding to Unit S.IV is distinguished from Units S.IA and S.IB by a decrease in biogenic elements and an increase in the terrigeneous ma-

F5. Seismic Line NS3, p. 23.

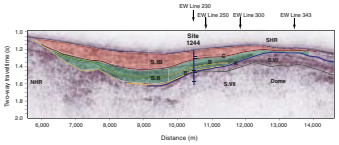

terial. It is also characterized by rapid deposition (~160 cm/k.y.) and a high frequency of locally derived turbidites generated by rapid changes in seafloor topography, which resulted in slope instability.

Structure

The primary structural features in the study area (shown on Fig. F4) are (1) Fault/Fold F, which represents landward-vergent deformation front during an earlier stage of development of Hydrate Ridge; (2) the "Dome," a broad uplift of Units S.VI and S.VII that has been intermittently active and now forms the core of Hydrate Ridge; (3) Anticlines A and B, which are localized uplifts of Units S.VI and S.VII; and (4) Fault System E, which forms the eastern boundary of the "Dome." In this section, we reconstruct the history of activity of these features through detailed examination of the topography of key unconformities and seismic stratigraphic patterns such as those shown in Figure F3.

Fold F and Faults F1 and F2

The most prominent fault-related fold (Fold F) deforms Unit S.IV and controls the geometry of Unit S.IV and S.III strata in the western part of the survey region (Fig. F4). The fold is a north-northeast-striking, doubly plunging fold (Fig. F6A), which may be cored by Fault F1 and probably developed because of drag along Fault F2 (Fig. F4A). The seismic survey encompasses only its northern half, which is plunging by ~3°. The interpretation of Fold F as a thrust-cored, landward-vergent fold formed at the deformation front is based on (1) reconstruction of the fold's evolution inferred from the geometry of the strata (Fig. F6B), which suggests a thrust fold in the hanging wall and formation of a basin overlying the footwall of Fault F2, and (2) similarity to the imbricated, landward-vergent thrust faults studied by Flueh et al. (1998) on the accretionary prism offshore Washington, which have similar amplitude and wavelength to Fold F. Two splays (F1 and F2) of the deeper-rooted thrust fault system could be mapped. Splay F1 was inferred from the small interlimb angle of Fold F (Fig. F4A). Splay F2 is a conspicuous termination surface in the deeper stratigraphy (Fig. F4). It disrupts younger strata than does Splay F1, suggesting more recent activity than Splay F1.

The Dome and Anticlines A and B

Middle to late Pleistocene slope-basin strata lap onto a large dome-shaped feature (which we call the Dome) composed of Units S.VII and S.VI. The top of this feature was mapped and is referred to as Unconformity K (Figs. F2, F4, F7). The relief on Unconformity K is much greater than the present-day seafloor relief, and the shape of the Dome is nearly circular, centered on the present-day southern summit (Fig. F7). The 2-D lines suggest an even more pronounced bulge beneath northern Hydrate Ridge. A secondary elongated bulge on the eastern flank of the Dome is referred to as Anticline A. Anticline A has a distinct topographic signature at present. Both the Dome and Anticline A are characterized by onlapping of the overlying strata against the paleorelief (Fig. F8E). Relatively rapid growth of the Dome at ~1.0 Ma is inferred from the abrupt pinching-out of Unit S.III to the east (Fig. F4, F8A). Units S.VI and S.VII are too deformed to reconstruct the early evolution of the Dome.

F6. Map of Horizons A′ and A, p. 24.

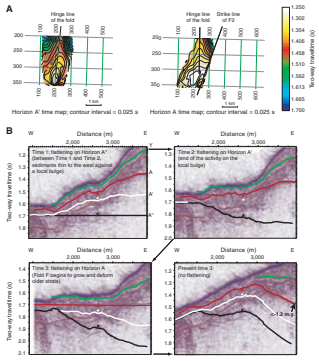

F7. Time map to Unconformity K, p. 25.

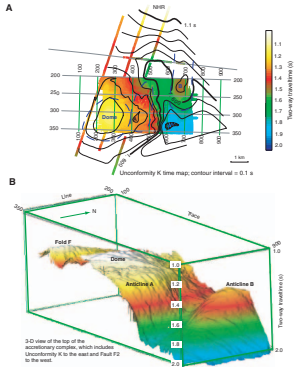

F8. Isopach maps of Units S.III, S.II, S.IB, and S.IA, p. 26.

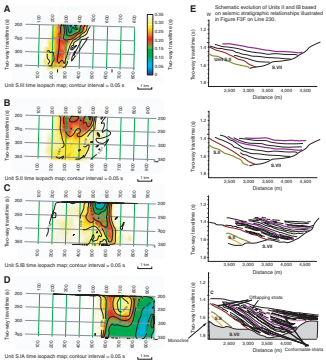

Anticline B (Fig. F4A–F4B), in the northeast part of the survey region, has only a slight signature in the topography but represents dramatic topography on Unconformity K (Fig. F7). Progressive fanning of the strata of Unit S.IV on the eastern flank of Anticline B suggests that the major growth period of the feature occurred at 1.0 to 0.3 Ma (Fig. F2). A sharp unconformity at the top of Unit S.IV indicates that Anticline B represented a bathymetric high ~0.2 m.y. ago, which is the minimum age of Unit S.IB. The progressive tilting and bending of Units S.II and S.IB and onlap of these onto the flanks of Anticline B suggest progressive subsidence of the feature relative to the Dome and eventual burial by Unit S.IA since ~0.2 Ma. This is probably a result of reinitiation of uplift of the Dome at ~0.3 Ma. This stage of uplift probably continues at present.

Syn- and Posttectonic Deformation Recorded within Unit S.II Strata

Contours on the time map of Horizon B, located within Unit S.II, show an anticline plunging to the north-northeast; the fold is slightly asymmetrical, with the northeast limb dipping more steeply than the western limb (Fig. F9A). The hinge line of the fold corresponds to the crest of SHR and lies slightly to the east of and approximately parallel to Fault F2 where defined by Horizon A, suggesting continuing thrusting on Fault F2 through at least the time of deposition of Unit S.II. The eastern limb of the fold is more prominent and is disrupted by clear north-south-striking normal faults that extend to the seafloor (Fig. F10B). Thickening of the interval between the stratigraphic Horizons B and B′ on the downdropped side of the faults (Fig. F9B) suggests synsedimentary faulting.

Fault System E

A deeply buried normal fault system accommodates the subsidence of the eastern basin relative to SHR. Two north-south-striking fault-splays are shown on Figure F4C and F4D. The offsets of the faults average ~0.2 s and sum to a total offset of 0.5 s (~387 m) in Unit S.VI in the southern part of the survey. Offset decreases to zero to the north, where these faults are no longer imaged (Fig. F4A). It is possible, however, that the vertical offsets observed in Figure F4C and F4D are the result of wrench faulting along a strike-slip fault system. The maximum offset of 600 m recorded during the 3-D survey precludes imaging of a steeply-dipping strike-slip fault where there is no significant component of dip-slip displacement.

The geometry of Units S.IA and S.IB, which are draped over Fault System E, suggests syndeformation sedimentation accompanying uplift of the Dome. This can be interpreted to result from either rapid uplift of the Dome since 0.3 Ma in response to underplating and duplexing of oceanic crust and sediments at depth (Tréhu et al., this volume), from clockwise block rotation of Hydrate Ridge, which would result in downdrop of the basin relative to the Dome (Johnson et al., this volume), or from a a combination of these mechanisms.

F9. Time map to Horizon B and seismic data from Line 230, p. 27.

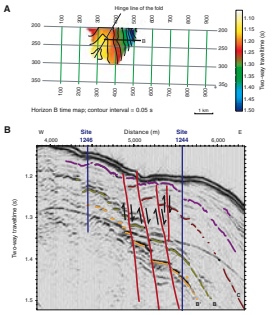

F10. Sequence of reconstructed cross sections, p. 28.

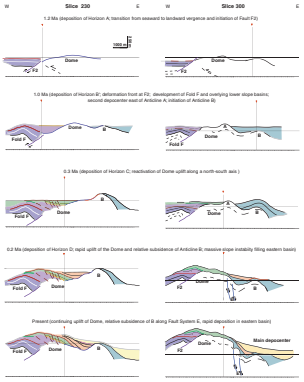

TECTONIC HISTORY OF SOUTHERN HYDRATE RIDGE

Figure F10 summarizes the tectonic history of SHR as inferred from the stratigraphic and structural interpretations presented in "Interpretation of Seismic Units and Structures," p. 5. This reconstruction was achieved by sequential removal of the effects of sedimentation and deformation. Structures of interest were unfolded by sequential flattening of key horizons, resulting in the geometric adjustment of overlying layers. The changes in geometry of the overlying layers through time were then used to indicate the timing of various folds throughout the region. Plane strain was assumed, allowing application of the constant bed length and the constant area rules. Some unit boundaries had to be approximated, for they are poorly constrained by the data. Horizontal original bedding was assumed except in cases of clear buttress unconformities associated with Anticline B and Fault System E. We also interpreted the absence of depositional sequences to be evidence for paleobathymetric highs that either impeded the deposition or caused slope failure events. The cross sections correspond to east-west Lines 230 (Fig. F4A) and 300 (Fig. F4C) from the 3-D survey. These two lines cut across most of the ODP sites, maximizing temporal constraints. Line 230 represents the northern part of the survey area where the slope basins formed by Units S.III, S.II, and S.IB are prominent and provides detailed information on the late Pleistocene geology. Line 300 crosses the shallowest part of Fold F and the Dome and provides better resolution for the tectonic reconstruction of early Pleistocene events. Comparison of the sections illustrates the important north-south variations within the survey area.

Late Pliocene sediments originally deposited as part of the deep-sea Astoria abyssal fan occur in the core of the proto-Dome (Unit S.VII), which was probably formed at the toe of the accretionary complex overlying a seaward-verging frontal thrust (Johnson et al., this volume). Rapid deposition of Astoria Fan sediments at the base of the slope continued in the early Pleistocene with deposition of Unit S.V. Simultaneously, sediments of Unit S.VI were deposited on the lower slope, albeit at a slow rate. Glauconite-rich layers recovered at Sites 1251 and 1252 near the top of Unit S.VII and within Unit S.VI support the inference of very slow sedimentation in the eastern part of the study region during this time period (Shipboard Scientific Party, 2003e). The wavy and chaotic seismic character of Unit S.VI suggests pervasive compressional deformation throughout the proto-Dome during this time period, but the details are not well determined.

Sometime between the deposition of Horizon A′ and Horizon A, (~1.2 m.y., based on biostratigraphy), the vergence of thrusting at the deformation front changed to landward, which thrust sediments of Unit S.V over the older sediments of Unit S.VII along Fault F2. The upper panels of Figure F10 depict this transition. Development of Fault F2 was accompanied by development of a drag fold, Fold F, creating a basin that was filled by sediments of Unit S.III. This model is supported by the linear character and north-south strike of the hinge line of Fold F, indicating east-west strain.

Fold F was active throughout deposition of Unit S.III, as indicated by the divergence of the strata on the flanks of the fold (Figs. F4, F6). Analysis of the internal geometry of onlap and truncation of strata within Unit S.III indicates that three paleobathymetric highs controlled the

distribution of Unit S.III: Fold F to the west, the Dome to the south, and Anticline A to the east. This episode of sedimentation extended from ~1.0 to ~0.5 Ma, although timing of the transition from Unit S.III to S.II is poorly constrained. Inconsistencies between mapping of coherent seismic sequences and biostratigraphic constraints during this time period may be due to redeposition of sediments shed from the topographic highs because of slope instability. This pattern of sedimentation continued from ~0.5 to ~0.3 Ma with deposition of Unit S.II. As Anticline B grew relative to Anticline A, it became the eastern boundary structure of the basin in which Unit S.II was deposited.

Biostratigraphic data indicate that sediments of Unit S.IV, which are found on the eastern and southern flanks of Anticline B, are coeval with Units S.III and S.II. The strata of Unit S.IV are divergent as the result of the synsedimentary activity of Anticline B and unconformably overlie S.VII strata at a very small angle (Fig. **F4**), indicating low relief of Anticline B at 1.0 Ma and major uplift soon after 1.0 Ma, during the deposition of Unit S.IV. Uplift of Anticline B appears to have stopped relative to the Dome since 0.3 Ma, as the eastern basin was filled with Units S.IA and S.IB. The lapping onto and thinning of Unit S.II on the western flank of Anticline B and the rapid deposition of coeval Unit S.IV on the eastern flank suggest that either there was a continuous high between Anticline A and Anticline B that did not provide any accommodation space for sediment deposition in this region or that one or more major slope collapses occurred between 1.0 and 0.3 Ma along Horizon K on the northern flank of Anticline A. The latter would also explain the sudden truncation of Unit S.VI strata to the north as observed on 2-D Line NS3 (Fig. **F5**).

Unit S.IV strata are truncated at the erosion Surface U (Fig. **F4**), indicating another major erosion event at ~0.3 Ma. Because the erosion surface is currently dipping to the south and there is no indication for a tilt of the strata to the south, we suggest that the Event U corresponds to a slope failure along the southern flank of Anticline B that truncated Unit S.IV. This event possibly occurred during the final stage of uplift of Anticline B. That Anticline B has been inactive since ~0.2 Ma is indicated by onlap of Unit S.IA.

The northeastern migration of uplift from Anticline A to Anticline B is enigmatic, since the deformation front was probably migrating west during this time as sediment was accreted. The abrupt southern termination of the Anticline B uplift is also difficult to explain in the context of a north-south-trending subduction zone. We speculate that uplift followed by subsidence may have been due to subduction of a topographic feature riding on the Juan de Fuca plate. Flemings and Tréhu (1999) inferred the presence of a deeply subducted ridge or chain of seamounts beneath the upper slope of the Cascadia subduction zone from 42° to 44°N based on modeling of gravity and magnetic data. If this buried structure is attached to the subducting plate, it would have been beneath the crest of Hydrate Ridge at ~1 Ma and would have moved northeast relative to the upper plate. Subduction of seamounts is known to have a impact on the structure of the continental margin offshore Central America (e.g., Ranero and von Huene, 2000; von Huene et al., 2000) and Nankai (e.g., Park et al., 2004). In this model, the first episode of uplift of the Dome (~1 Ma) and the uplift of Anticline B are attributed to passage of the subducted ridge. Both of these episodes of uplift were followed by sedimentation over the crest of the former topographic high, consistent with collapse of the margin in the wake of the subducted ridge.

Reactivation of uplift of Unit S.VII along the present-day axis of Hydrate Ridge since ~0.3 Ma is inferred based on eastward migration of the depocenter for Units S.II and S.IB (Fig. F8). This uplift along a north-south axis was accompanied by normal faulting in Unit S.II. We interpret this to be due to a reinitiation of seaward-vergent thrusting farther to the west accompanied by underthrusting of sediment and formation of deeply buried sediment duplexes at depth beneath Hydrate Ridge (Tréhu et al., this volume).

The development of Fault System E, which disrupts Unit S.VI beneath the southeastern flank of SHR, is the most recent structural feature we discuss. Offlapping of the Unit S.IB strata shows an increase in the uplift rate relative to the sedimentation rate since ~0.2 Ma. Within Unit S.IB, the increased abundance of the pelagic sediments with time is observed (Shipboard Scientific Party, 2003b). This is interpreted to result from the isolation of the top of the ridge as it is uplifted out of the region of turbidity current deposition and into a regime of pelagic drape sedimentation. An increase in dip of the strata within Unit S.IA with time and the two debris flow deposits (DBF1 and DBF2 on Fig. F4), as well as the thinning of the beds against the flanks of the Dome provide evidence for the ongoing relative subsidence of the eastern basin during the deposition of Unit S.IA. This may be due to rotation of Hydrate Ridge in a clockwise direction, with extension in the basin adjacent to southern end of the ridge, as discussed by Johnson et al. (this volume).

IMPACT OF STRATIGRAPHIC AND STRUCTURAL HISTORY ON GAS HYDRATE DISTRIBUTION

Gas hydrates form when methane-rich fluids enter the GHSZ. At SHR, the distribution of gas hydrates is highly heterogeneous (Tréhu et al., 2004a). Generally, gas hydrate comprises <5% of the pore space, averaged over the GHSZ. However, massive gas hydrate deposits, estimated to comprise ~25% of the total volume, are present in the upper 20–30 m at the summit of the ridge. Very little hydrate (<2% of pore space) was found within the sediments of the eastern basin, except for immediately above the base of the GHSZ. We note that no drilling was permitted at the crest of Anticline B. In this section, we discuss how the geologic history outline in the previous sections has influenced large-scale patterns in gas hydrate distribution.

The BSR is a conspicuous reflection with negative amplitude through most of the 3-D survey. Its amplitude, however, varies greatly. Figure F11 shows the variation in relative amplitude of the BSR overlain by the boundaries between the stratigraphic units on the BSR surface. It shows several distinct zones of high amplitude.

F11. Map of BSR amplitude, p. 29.

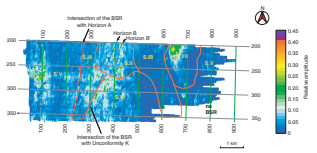

The most prominent high-amplitude anomaly is associated with the buried Anticline B and lies within Unit S.VII. We note that a drill site that was originally located on this anomaly was moved to Site 1252 by the ODP Pollution Prevention and Safety Panel. We interpret the relatively uniform character of this amplitude anomaly to indicate the widespread presence of free gas throughout these older, seismically incoherent, and presumably pervasively fractured sediments and relatively high and heterogeneous gas hydrate content within the GHSZ.

Another pronounced bright spot is located in sediments of Unit S.VI on the western flank of SHR. This bright spot is associated with the lo-

cal circular high that was active prior to deposition of Horizon A. This relict structure, which may have been a mud volcano in the trench, as is observed in subduction zones elsewhere, appears to remain as a preferential methane migration path ~1 Ma since it was active. No drilling data are available to test this hypothesis.

The summit region is characterized by a relatively large zone containing numerous linear and patchy bright spots in the tightly folded and deformed sediments of Unit S.VI. We interpret these patterns to reflect variable permeability controlled by discrete stratigraphic horizons and faults.

Where the base of the GHSZ falls in the younger sediments of Units S.III, S.II, and S.I, the BSR is generally faint or absent except where coarse-grained horizons like A, B, and B′ exist to provide paths for gas migration. Where these horizons intersect the BSR, strong anomalies are observed. These may, at least in part, indicate constructive interference between two negative polarity reflections. The numerous small normal faults that offset strata in Unit S.II may also contribute to the bright BSR and to relatively high and heterogeneous (1%–8%) gas hydrate content within the GHSZ (Tréhu et al., 2004a; Weinberger et al., 2005).

In summary, the strongest BSR anomalies are associated with the oldest sediments. We infer that these have the potential to deliver free gas to the GHSZ more readily than the younger strata for at least two reasons. First, these older sediments have generally undergone greater uplift, leading to a large decrease in the solubility of methane in the pore fluids because of depressurization. Based on the methane content of abyssal plain sediments drilled at Deep Sea Drilling Project (DSDP) Site 174, these sediments should be supersaturated in methane when uplifted to the depth at which they are now found (Claypool and Kaplan, 1974; **Claypool et al.,** this volume; **Tréhu et al.,** this volume). Second, pervasive fracturing of recovered samples, the variable character of geophysical logs from these zones, and very low gradients in chloride concentration (Shipboard Scientific Party, 2003b, 2003d, 2003e; Torres et al., 2004b) suggest that the accretionary complex sediments are permeable and that the pore fluid within them is well mixed, allowing efficient transport of gas into the GHSZ. We note that at northern Hydrate Ridge, where venting and authigenic carbonate development is widespread over the summit of the structure, sediments of Units S.VII and S.VI are present very near the surface, consistent with the association we document here of older sediments with venting. Our results also demonstrate the value of high-resolution seismic data in identifying relict buried structures within the older sediments that focus fluid flow.

CONCLUSIONS

We have reconstructed the geologic history of SHR using techniques adapted from seismic sequence stratigraphy and ages determined from biostratigraphic analysis of Leg 204 samples. Between 1.6 and 1.2 Ma, sediments from the abyssal plain were accreted to the margin along a seaward-vergent thrust fault. At ~1.2 Ma, vergence direction changed and Fault F2, a landward-vergent fault overlain by a drag fold (Fold F) thrust deep-sea fan sediments over the recently accreted sediments. This episode of landward vergence lasted to ~0.3 Ma. During this time period, uplift in the accretionary complex shifted toward the northeast, from Anticline A on the eastern flank of the present ridge to Anticline B, which is now buried beneath the sediments of the slope basin east of

Hydrate Ridge. This migrating uplift resulted in shifting depocenters and overlapping slope basins. Early to middle Pleistocene strata (Units S.IV, S.III, and S.II) of these basins consist of recycled abyssal plain sediments shed from the bathymetric highs and ponded into the depocenters. The cause of this northeastward shift in uplift while the deformation front migrated west remains enigmatic but may be related to passage of a ridge or seamount on the subducting plate. A second reorganization of the deformation front, to seaward thrusting farther to the west, began sometime prior to 0.3 Ma, probably resulting in reactivation of uplift of the modern Hydrate Ridge in response to sediment underplating and duplexing. Normal faulting in the slope basin sediments at the crest accompanied this phase, which likely continues today.

Because of this history, a wide range of lithologies currently falls within the gas hydrate stability zone at SHR. We note a correlation between BSR amplitude and sediment age, with high-amplitude BSR anomalies correlated with uplifts of the older, lithified, and fractured accreted sediments that were originally deposited on the abyssal plain. Gas to feed gas hydrate formation in these sediments is probably exsolved from pore water as a result of decreased gas solubility due to tectonic uplift. We infer that the gas migrates into the gas hydrate stability zone through pervasive fracture permeability in the accretionary complex and that gas migration and gas hydrate formation in the overlying slope basin sediments is limited to a few discrete permeable horizons or faults.

ACKNOWLEDGMENTS

We thank the crew of the *Thomas Thompson* for their efforts to maintain what must have seemed to them to be a strange track line while we were acquiring the 3-D seismic survey. We also thank John Diebold, Scholtz, Mark Weiderspahn, and Steffan Saustrup for keeping the GI guns, acquisition system, and data quality control hardware and software going. Finally, we thank the ODP staff and crew of the *JOIDES Resolution* for a job well done. This research used samples and/or data provided by the Ocean Drilling Program (ODP). ODP is funded by the U.S. National Science Foundation (NSF) and participating countries under management of Joint Oceanographic Institutions (JOI), Inc. Acquisition and analysis of the seismic data were funded by grants to OSU (JOI-U.S. Science Support Program [USSSP] F01558, NSF OCE-9907205, and NSF OCE-0002410) and to UTIG (NSF OCE-9907205). Data processing was performed using Kingdom Suite software donated to OSU by Seismic Micro-Technology, Inc.

REFERENCES

Arsenault, M.A., Tréhu, A.M., Bangs, N., and Nakamura, Y., 2001. *P*-wave tomography of Hydrate Ridge, Oregon continental margin. *Eos, Trans. Am. Geophys. Union,* 82:604. (Abstract).

Bangs, N.L.B., Musgrave, R.J., and Tréhu, A.M., 2005. Upward shifts in the southern Hydrate Ridge gas hydrate zone following postglacial warming, offshore Oregon. *J. Geophys. Res.,* 110(B3):B03102. **doi:10.1029/2004JB003293**

Bohrmann, G., Greinert, J., Suess, E., and Torres, M., 1998. Authigenic carbonates from the Cascadia subduction zone and their relation to gas hydrate stability. *Geology,* 26(7):647–650. **doi:10.1130/0091-7613(1998)026<0647:ACFTCS>2.3.CO;2**

Burbank, D.W., and Vergés, J., 1994, Reconstruction of topography and related depositional systems during active thrusting. *J. Geophys. Res.,* 99(B10):20281–2029. **doi:10.1029/94JB00463**

Chevallier, J., 2004. Seismic sequence stratigraphy and tectonic evolution of southern Hydrate Ridge [M.S. thesis]. Oregon State Univ., Corvallis.

Claypool, G.E., and Kaplan, I.R., 1974. The origin and distribution of methane in marine sediments. *In* Kaplan, I.R. (Ed.), *Natural Gases in Marine Sediments:* New York (Plenum), 99–139.

Fleming, S.W., and Tréhu, A.M., 1999. Crustal structure beneath the central Oregon convergent margin from potential field modeling: evidence for a buried basement ridge in local contact with a seaward dipping backstop. *J. Geophys. Res.,* 104(B9):20431–20449. **doi:10.1029/1999JB900159**

Flueh, E.R., Fisher, M.A., Bialas, J., Childs, J.R., Klaeschen, D., Kukowski, N., Parsons, T., Scholl, D.W., Ten Brink, U., Tréhu, A.M., and Vidal, N., 1998. New seismic images of the Cascadia subduction zone from Cruise SO108—ORWELL. *Tectonophysics,* 293(1–2):69–84. **doi:10.1016/S0040-1951(98)00091-2**

Goldfinger, C., Kulm, L.D., Yeats, R.S., Applegate, B., Mackay, M., and Cochrane, G.R., 1996. Active strike-slip faulting and folding of the Cascadia plate boundary and forearc in central and northern Oregon. *In* Rogers, A.M., Walsh, T.J., Kockelman, W.J., and Priest, G. (Eds.), *Assessing and Reducing the Risk of Earthquake Hazards in the Pacific Northwest.* U.S. Geol. Surv. Prof. Pap., 1560:223–256.

Johnson, J.E., Goldfinger, C., and Suess, E., 2003. Geophysical constraints on the surface distribution of authigenic carbonates across the Hydrate Ridge region, Cascadia margin. *Mar. Geol.,* 202(1–2):79–120. **doi:10.1016/S0025-3227(03)00268-8**

MacKay, M.E., Moore, G.F., Cochrane, G.R., Moore, J.C., and Kulm, L.D., 1992. Landward vergence and oblique structural trends in the Oregon margin accretionary prism: implications and effect on fluid flow. *Earth Planet. Sci. Lett.,* 109(3–4):477–491. **doi:10.1016/0012-821X(92)90108-8**

McNeill, L.C., Goldfinger, C., Kulm, L.D., and Yeats, R.S., 2000. Tectonics of the Neogene Cascadia forearc basin: investigations of a deformed late Miocene unconformity. *Geol. Soc. Am. Bull.,* 112(8):1209–224. **doi:10.1130/0016-7606(2000)112<1209:TOTNCF>2.3.CO;2**

Milkov, A.V., Claypool, G.E., Lee, Y-J., Xu, W., Dickens, G.R., Borowski, W.S., and the ODP Leg 204 Scientific Party, 2003. In situ methane concentrations at Hydrate Ridge offshore Oregon: new constraints on the global gas hydrate inventory from an active margin. *Geology,* 31:833–836.

Milkov, A.V., Dickens, G.R., Claypool, G.E., Lee, Y-J., Borowski, W.S., Torres, M.E., Xu, W., Tomaru, H., Tréhu, A.M., and Schultheiss, P., 2004. Co-existence of gas hydrate, free gas, and brine within the regional gas hydrate stability zone at Hydrate Ridge (Oregon margin): evidence from prolonged degassing of a pressurized core. *Earth Planet. Sci. Lett.,* 222(3–4):829–843. **doi:10.1016/j.epsl.2004.03.028**

Mitchum, R.M., Jr., 1977. Seismic stratigraphy and global changes of sea level, Part 11. Glossary of terms used in seismic stratigraphy. *In* Payton, C.E. (Ed.), *Seismic Stratigraphy: Applications to Hydrocarbon Exploration.* AAPG Mem., 26:205–212.

Park, J.-O., Moore, G.F., Tsuru, T., Kodaira, S., and Kaneda, Y., 2004. A subducted oceanic ridge influencing the Nankai megathrust earthquake rupture. *Earth Planet. Sci. Lett.,* 217(1–2):77–84. **doi:10.1016/S0012-821X(03)00553-3**

Ranero, C.R., and von Huene, R., 2000. Subduction erosion along the Middle America convergent margin. *Nature (London, U. K.),* 404:748–752. doi:10.1038/35008046

Seely, D.R., Vail, P.R., and Walton, G.G., 1974. Trench slope model. *In* Burk, C.A., and Drake, C.L. (Eds.), *The Geology of Continental Margins:* Berlin (Springer-Verlag), 249–260.

Shipboard Scientific Party, 2003a. Explanatory notes. *In* Tréhu, A.M, Bohrmann, G., Rack, F.R., Torres, M.E., et al., *Proc. ODP, Init. Repts.,* 204: College Station, TX (Ocean Drilling Program), 1–102. **doi:10.2973/odp.proc.ir.204.102.2003**

Shipboard Scientific Party, 2003b. Site 1244. *In* Tréhu, A.M, Bohrmann, G., Rack, F.R., Torres, M.E., et al., *Proc. ODP, Init. Repts.,* 204: College Station, TX (Ocean Drilling Program), 1–132. **doi:10.2973/odp.proc.ir.204.103.2003**

Shipboard Scientific Party, 2003c. Site 1245. *In* Tréhu, A.M, Bohrmann, G., Rack, F.R., Torres, M.E., et al., *Proc. ODP, Init. Repts.,* 204: College Station, TX (Ocean Drilling Program), 1–131. **doi:10.2973/odp.proc.ir.204.104.2003**

Shipboard Scientific Party, 2003d. Site 1251. *In* Tréhu, A.M, Bohrmann, G., Rack, F.R., Torres, M.E., et al., *Proc. ODP, Init. Repts.,* 204: College Station, TX (Ocean Drilling Program), 1–119. **doi:10.2973/odp.proc.ir.204.110.2003**

Shipboard Scientific Party, 2003e. Site 1252. *In* Tréhu, A.M, Bohrmann, G., Rack, F.R., Torres, M.E., et al., *Proc. ODP, Init. Repts.,* 204: College Station, TX (Ocean Drilling Program), 1–62. **doi:10.2973/odp.proc.ir.204.111.2003**

Snavely, P.D., Jr., 1987. Tertiary geologic framework, neotectonics, and petroleum potential of the Oregon-Washington continental margin. *In* Scholl, D.W., Grantz, A., and Vedder, J.G. (Eds.), *Geology and Resource Potential of the Continental Margin of Western North America and Adjacent Ocean Basins—Beaufort Sea to Baja California.* Circum-Pac. Counc. Energy Miner. Resour., Earth Sci. Ser., 6:305–336.

Suess, E., Torres, M.E., Bohrmann, G., Collier, R.W., Rickert, D., Goldfinger, C., Linke, P., Heuser, A., Sahling, H., Heeschen, K., Jung, C., Nakamura, K., Greinert, J., Pfannkuche, O., Tréhu, A., Klinkhammer, G., Whiticar, M.J., Eisenhauer, A., Teichert, B., and Elvert, M., 2001. Sea floor methane hydrates at Hydrate Ridge, Cascadia margin. *In* Paull, C.K., and Dillon, W.P. (Eds.), *Natural Gas Hydrates: Occurrence, Distribution, and Detection.* Geophys. Monogr., 124:87–98.

Torres, M.E., McManus, J., Hammond, D.E., de Angelis, M.A., Heeschen, K.U., Colbert, S.L., Tryon, M.D., Brown, K.M., and Suess, E., 2002. Fluid and chemical fluxes in and out of sediments hosting methane hydrate deposits on Hydrate Ridge, OR. I: hydrological provinces. *Earth Planet. Sci. Lett.,* 201(3–4):525–540. **doi:10.1016/S0012-821X(02)00733-1**

Torres, M.E., Teichert, B.M.A., Tréhu, A.M., Borowski, W., and Tomaru, H., 2004. Relationship of pore water freshening to accretionary processes in the Cascadia margin: fluid sources and gas hydrate abundance. *Geophys. Res. Lett.,* 31:L22305. **doi:10.1029/2004GL021219**

Torres, M.E., Wallmann, K., Tréhu, A.M., Bohrmann, G., Borowski, W.S., and Tomaru, H., 2004. Gas hydrate growth, methane transport, and chloride enrichment at the southern summit of Hydrate Ridge, Cascadia margin off Oregon. *Earth Planet. Sci. Lett.,* 226(1–2):225–241. **doi:10.1016/j.epsl.2004.07.029**

Tréhu, A.M., and Bangs, N., 2001. 3-D seismic imaging of an active margin hydrate system, Oregon continental margin, report of Cruise TTN112. *Oregon State Univ. Data Rpt.,* 182.

Tréhu, A.M., Bohrmann, G., Rack, F.R., Torres, M.E., et al., 2003. *Proc. ODP, Init. Repts.,* 204: College Station, TX (Ocean Drilling Program). **doi:10.2973/odp.proc.ir.204.2003**

Tréhu, A.M., Flemings, P.B., Bangs, N.L., Chevallier, J., Gràcia, E., Johnson, J.E., Liu, C.-S., Liu, X., Riedel, M., and Torres, M.E., 2004a. Feeding methane vents and gas hydrate deposits at south Hydrate Ridge. *Geophys. Res. Lett.,* 31:L23310. **doi:10.1029/2004GL021286**

Tréhu, A.M., Long, P.E., Torres, M.E., Bohrmann, G., Rack, F.R., Collett, T.S., Goldberg, D.S., Milkov, A.V., Riedel, M., Schultheiss, P., Bangs, N.L., Barr, S.R., Borowski, W.S., Claypool, G.E., Delwiche, M.E., Dickens, G.R., Gracia, E., Guerin, G., Holland, M., Johnson, J.E., Lee, Y.-J., Liu, C.-S., Su, X., Teichert, B., Tomaru, H., Vanneste, M., Watanabe, M., and Weinberger, J.L., 2004b. Three-dimensional distribution of gas hydrate beneath southern Hydrate Ridge: constraints from ODP Leg 204. *Earth Planet. Sci. Lett.,* 222(3–4):845–862. **doi:10.1016/j.epsl.2004.03.035**

Tréhu, A.M., Torres, M.E., Moore, G.F., Suess, E., and Bohrmann, G., 1999. Temporal and spatial evolution of a gas-hydrate-bearing accretionary ridge on the Oregon continental margin. *Geology,* 27(10):939–942.

Tryon, M.D., Brown, K.M., and Torres, M.E., 2002. Fluid and chemical flux in and out of sediments hosting methane hydrate deposits on Hydrate Ridge, OR. II: hydrological processes. *Earth Planet. Sci. Lett.,* 201(3–4):541–557. **doi:10.1016/S0012-821X(02)00732-X**

von Huene, R., Ranero, C.R., Weinrebe, W., and Hinz, K., 2000. Quaternary convergent margin tectonics of Costa Rica, segmentation of the Cocos plate, and Central American volcanism. *Tectonics,* 19(2):314–334. **doi:10.1029/1999TC001143**

Weinberger, J.L., Brown, K.M., and Long, P.E., 2005. Painting a picture of gas hydrate distribution with thermal images. *Geophys. Res. Lett.,* 32(4):L04609. **doi:10.1029/2004GL021437**

Figure F1. A. Location of Hydrate Ridge in the Cascadia accretionary complex. The path of sediments from the Columbia River, which form the Astoria Fan and fill the subduction zone trench, is also shown (blue arrow). Deep Sea Drilling Project (DSDP) Sites 174 and 175 originally documented the influence of the Astoria Fan on development of the accretionary complex. **B.** Detailed bathymetric map of the accretionary complex in the vicinity of Hydrate Ridge. This part of the accretionary complex is characterized by strong along-strike variability in topography, in contrast to the region to the north, which is characterized by long, linear ridges. The location of ODP Site 892, drilling on northern Hydrate Ridge in 1992, and the limits of the 3-D seismic survey discussed in this paper are shown. SHR = southern Hydrate Ridge. **C.** Detailed topographic map in the vicinity of the 3-D seismic survey. Contour interval is 20 m. Locations of drill sites for Leg 204 and the position of seismic lines shown in this paper are shown. Line numbers within the 3-D volume extend from 200 at the northern edge of the survey to 350 at the southern edge and from 100 at the western edge to 833 at the eastern edge. MBARI - Monterey Bay Aquarium Research Institute. **D.** Depth-converted seismic section from the site survey for Leg 146 (**Tréhu et al.,** this volume). Box shows area detailed in Figure **F4A,** p. 21.

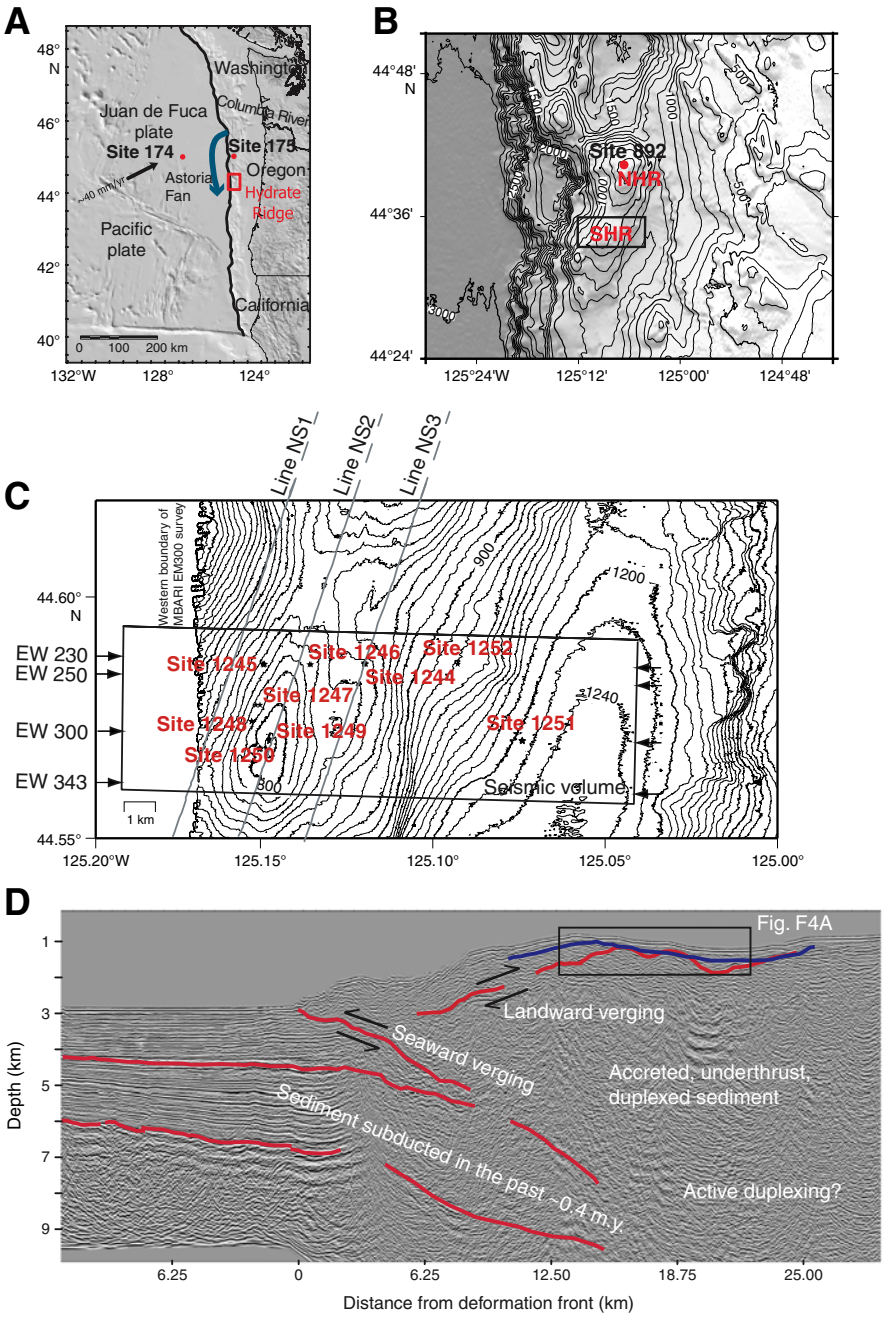

Figure F2. Comparison of lithologic units defined by the shipboard sedimentologists during Leg 204 (Shipboard Science Party, 2003a) with the seismic units defined in this paper. Lithologic units are shown as columns at each site. Ages determined by shipboard paleontologists, in millions of years, are shown as red numbers along the sides of the lithologic columns. Ages in parentheses are not compatible with the seismic data and are attributed to reworking of older sediments. Seismic stratigraphic units represent coherent sediment packages that can be mapped between sites and are labeled as Unit S.VII to S.IA. These are separated by seismic stratigraphic Horizons A, B, B′, C, D, and Y and major angular unconformities K and U. The position of significant structures (Anticlines A and B; Fold F; Faults F1, F2, and E; and the "Dome") and of the bottom-simulating reflection (BSR) are also shown.

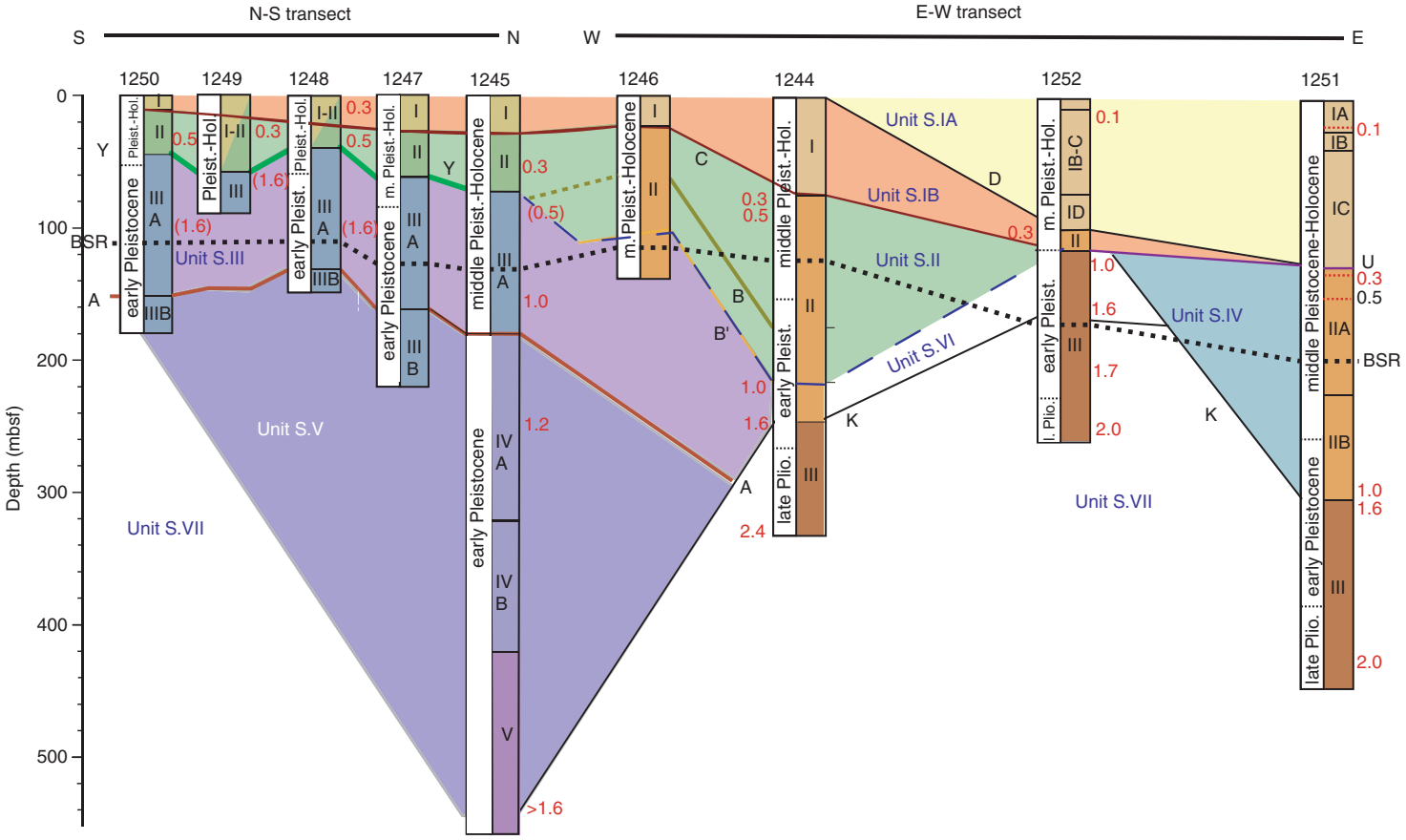

Figure F3. A. Nomenclature for growth strata deposited during thrust folding. **B–E.** Model of overlap, offlap, and onlap. Predictable geometries of syntectonic strata result from different ratio between the relative rates of crestal uplift and coeval sedimentation rates. Crestal uplift is measured with respect to either the base of the syntectonic strata adjacent to the fold or the position of the correlative marker beds found in both the anticline and the adjacent syncline. (B) When rates of accumulation are consistently greater than the rate of crestal uplift, overlap will occur. (C) Lower rates of accumulation versus uplift lead to offlap. (D) Reversals in the relative magnitude of these rates cause a switch in the bedding geometry. (E) Onlap occurs following offlap and a change to more rapid accumulation rates (A–E modified from Burbank and Verges, 1994). (Continued on next page.)

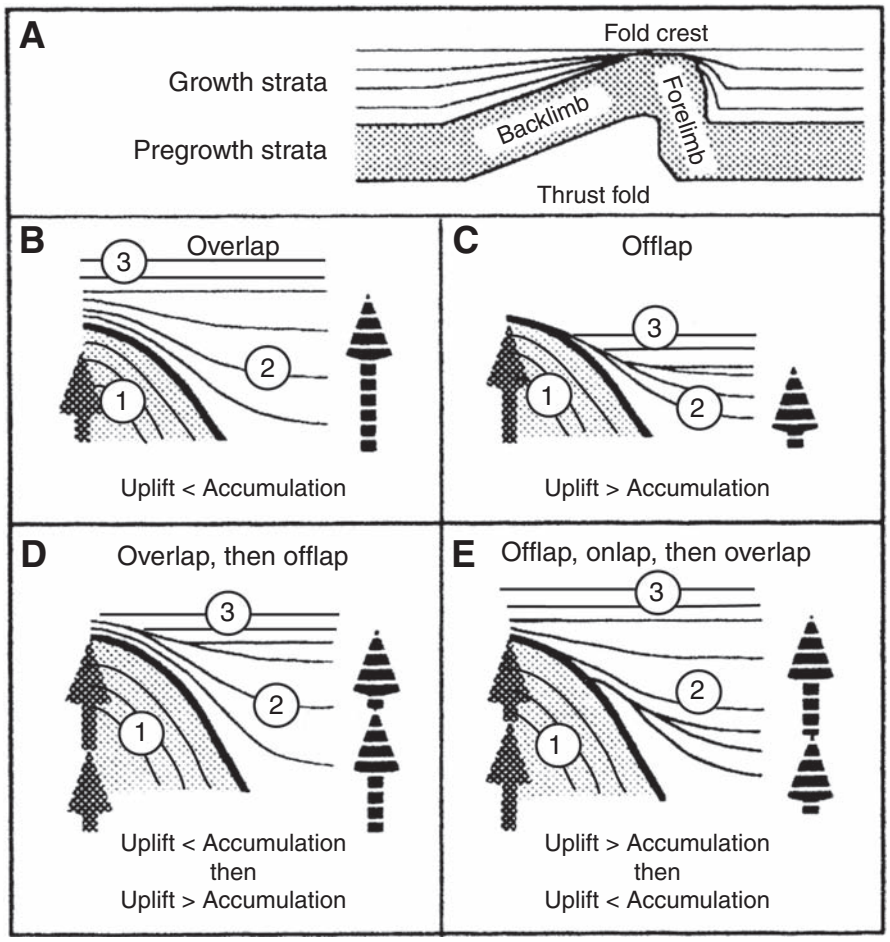

Figure F3 (continued). F. Examples of these characteristic seismic stratigraphic patterns in the 3-D data from southern Hydrate Ridge. BSR = bottom-simulating reflection.

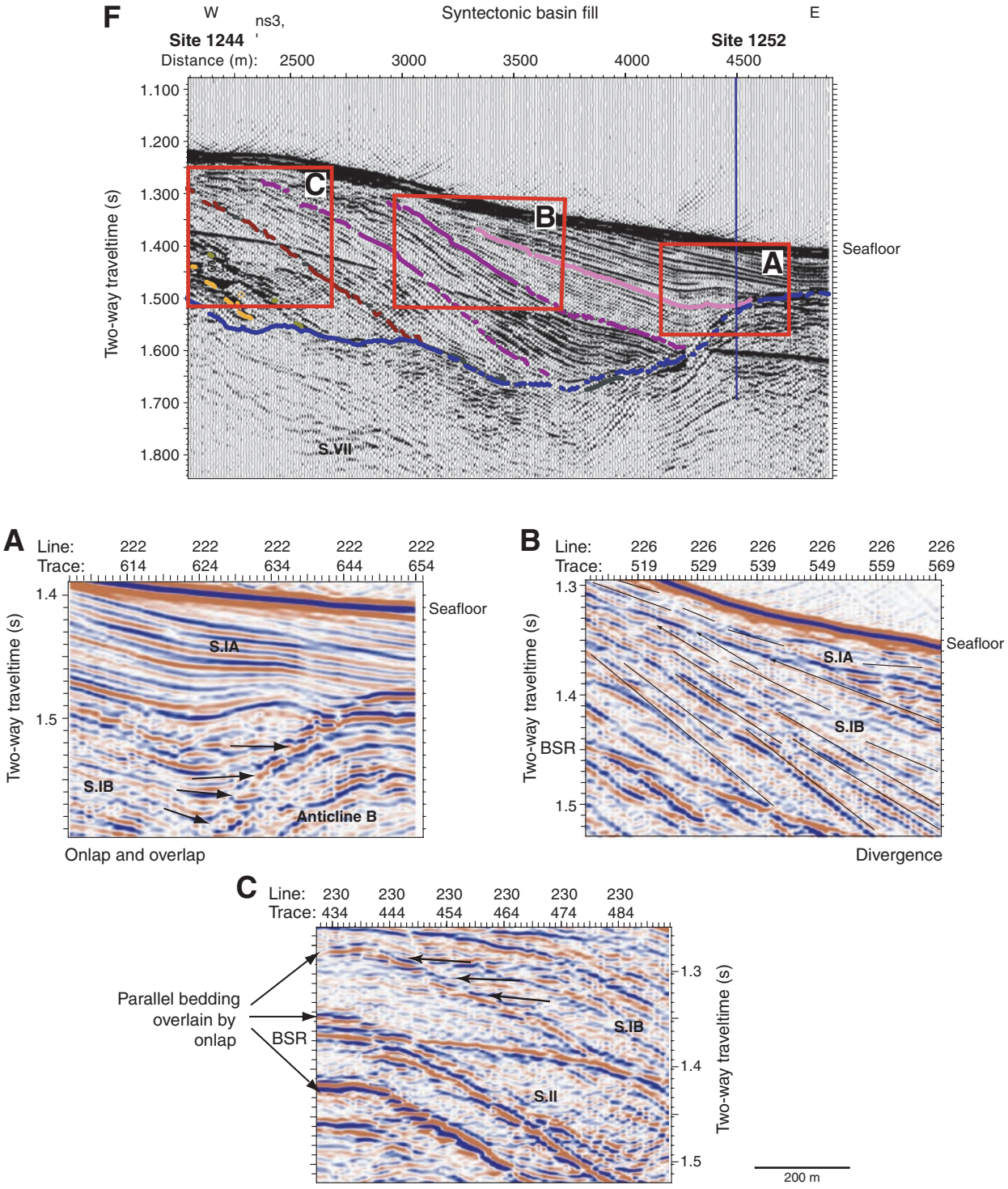

Figure F4. A, B. East-west slices through the 3-D seismic volume. Overlays show seismic stratigraphic units. Color code and letters to identify seismic units are the same as in Figure F2, p. 18, which shows correlation of seismic units with lithologic units and biostratigraphic ages. Important structural features are also labeled and identified as in Figure F2, p. 18. The depth axis for A and B was derived from correlation with Site 1245. DBF = debris flow deposit. (Continued on next page.)

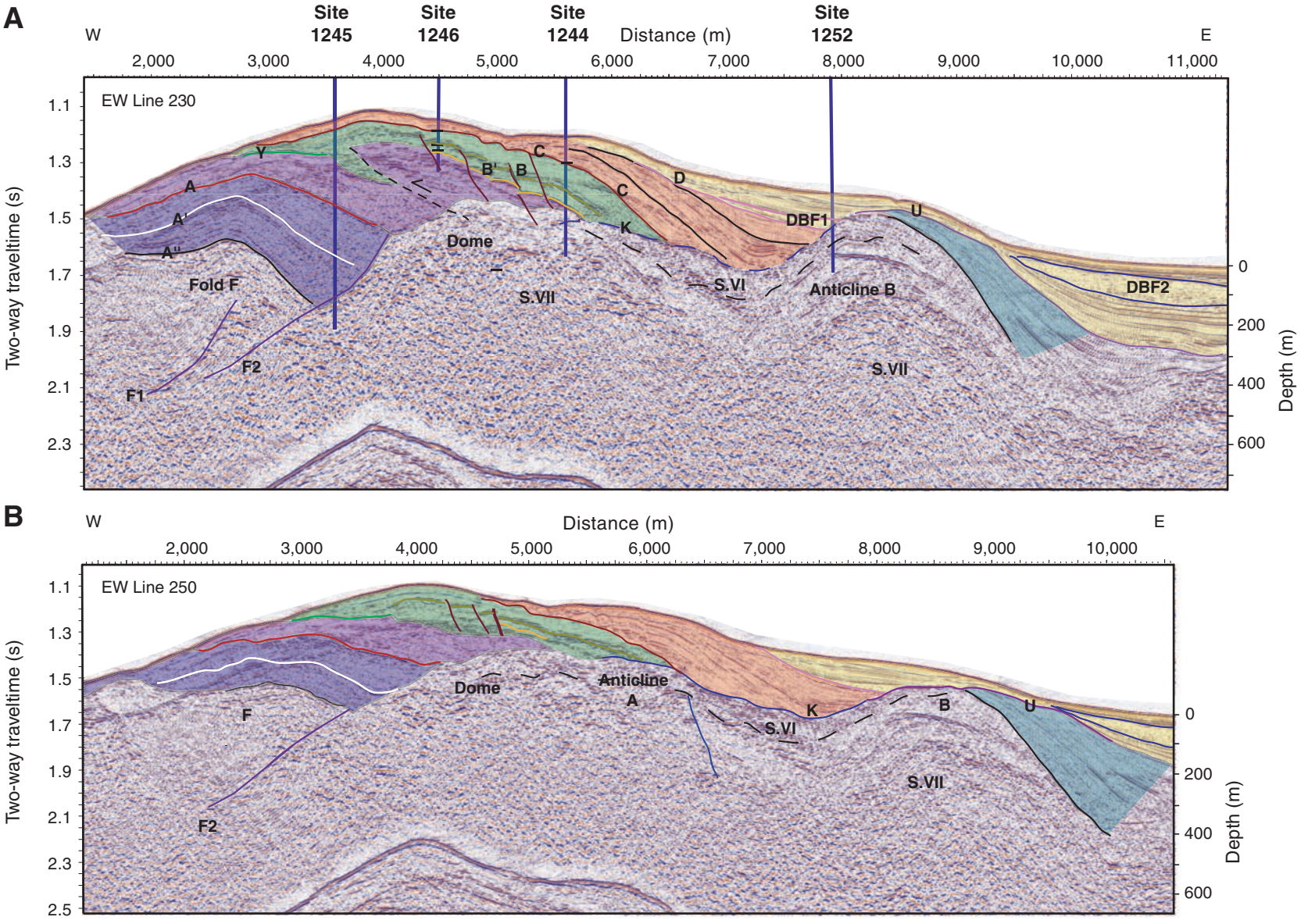

Figure F4 (continued). C, D. The depth axis on C and D was derived from Site 1251, Lines 300 and 343.

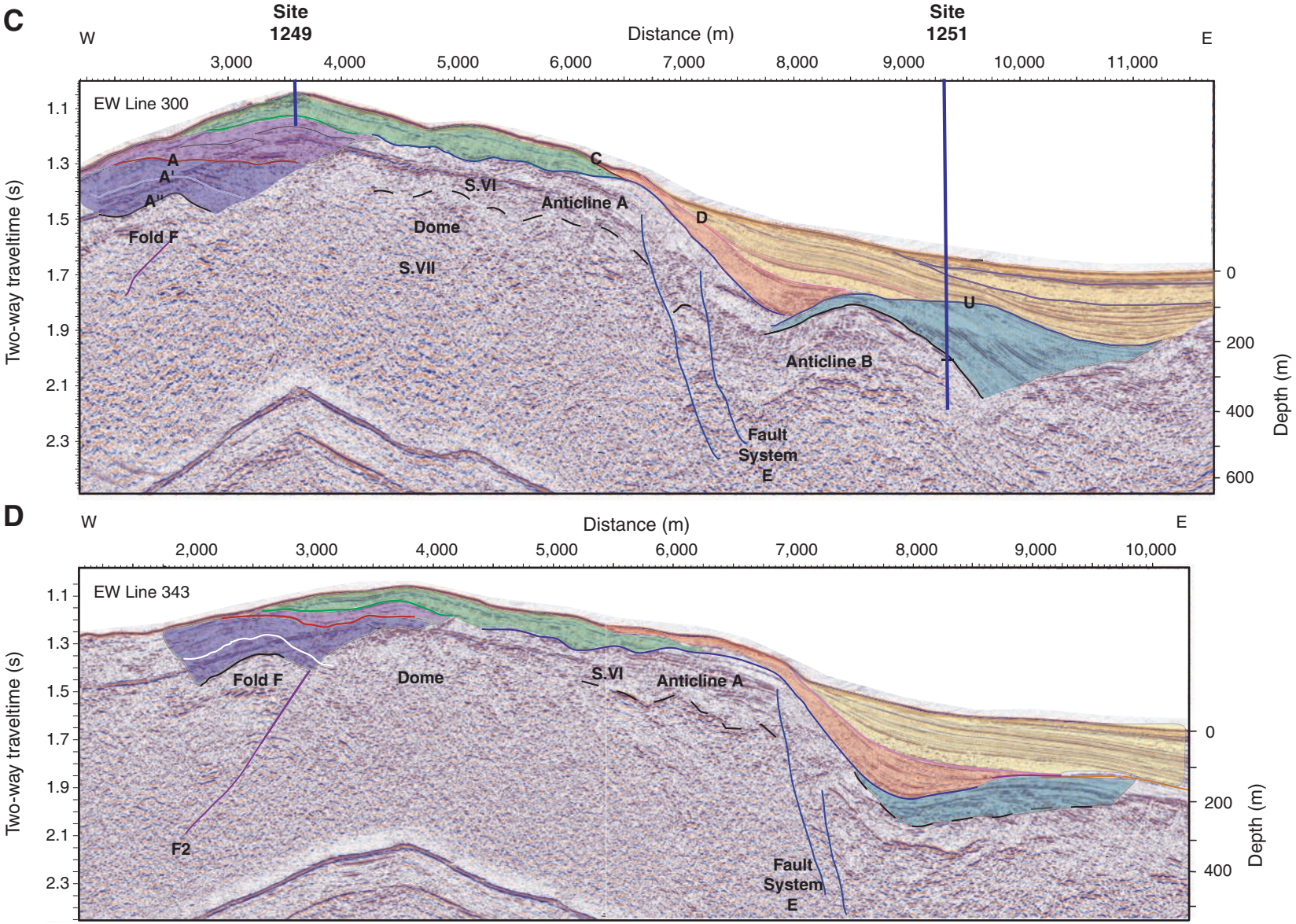

Figure F5. Seismic Line NS3 showing thinning of Units S.I and S.II toward the northern and southern summits of Hydrate Ridge. The location of this regional 2-D seismic profile is shown in Figure F1C, p. 17. NHR = northern Hydrate Ridge. SHR = southern Hydrate Ridge.

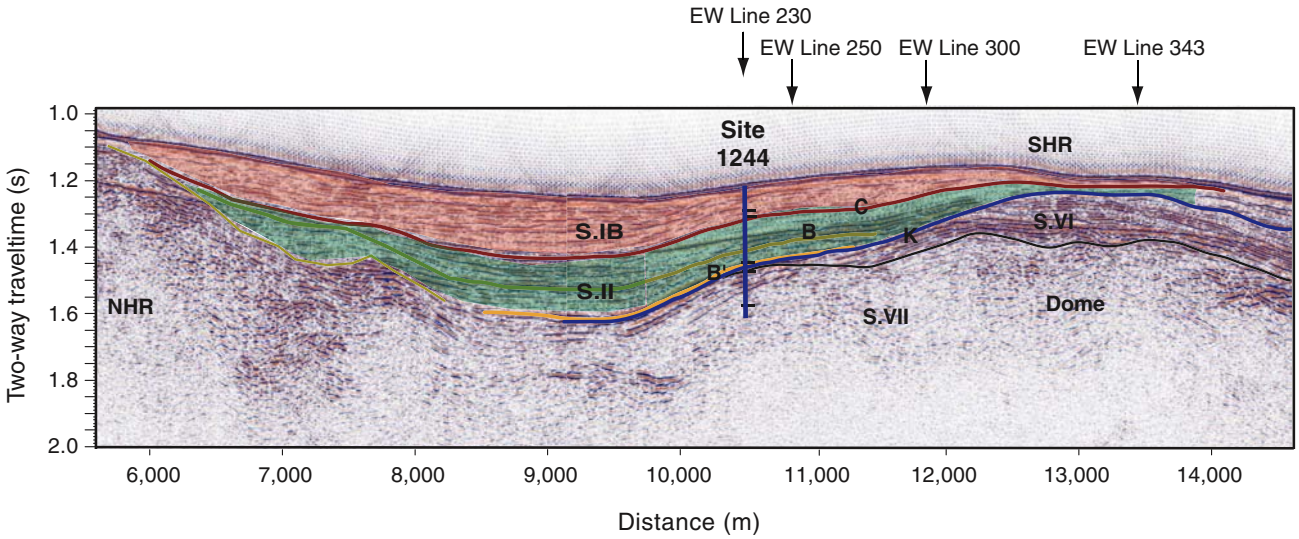

Figure F6. A. Map of Horizons A′ and A showing the strike of Fold F and Fault F2. **B.** Temporal evolution of Fold F shown by a series of seismic sections which have been progressively flattened on Horizons A″, A′, and A. That the presence of a local bulge active prior to ~1 Ma influences fluid flux at present is suggested by the large amplitudes beneath this structure and the large amplitude and slight relative uplift of the bottom-simulating reflection (BSR) here.

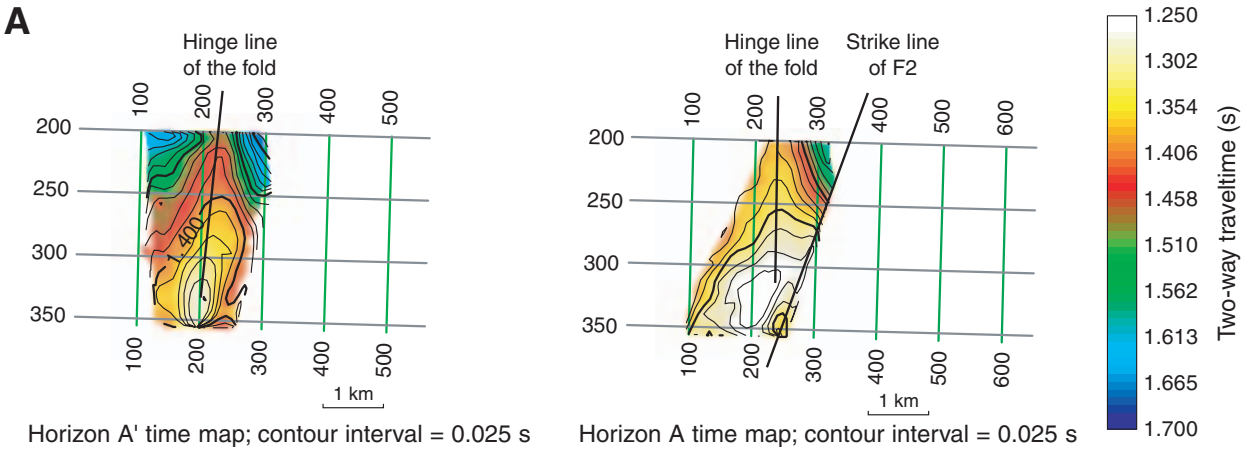

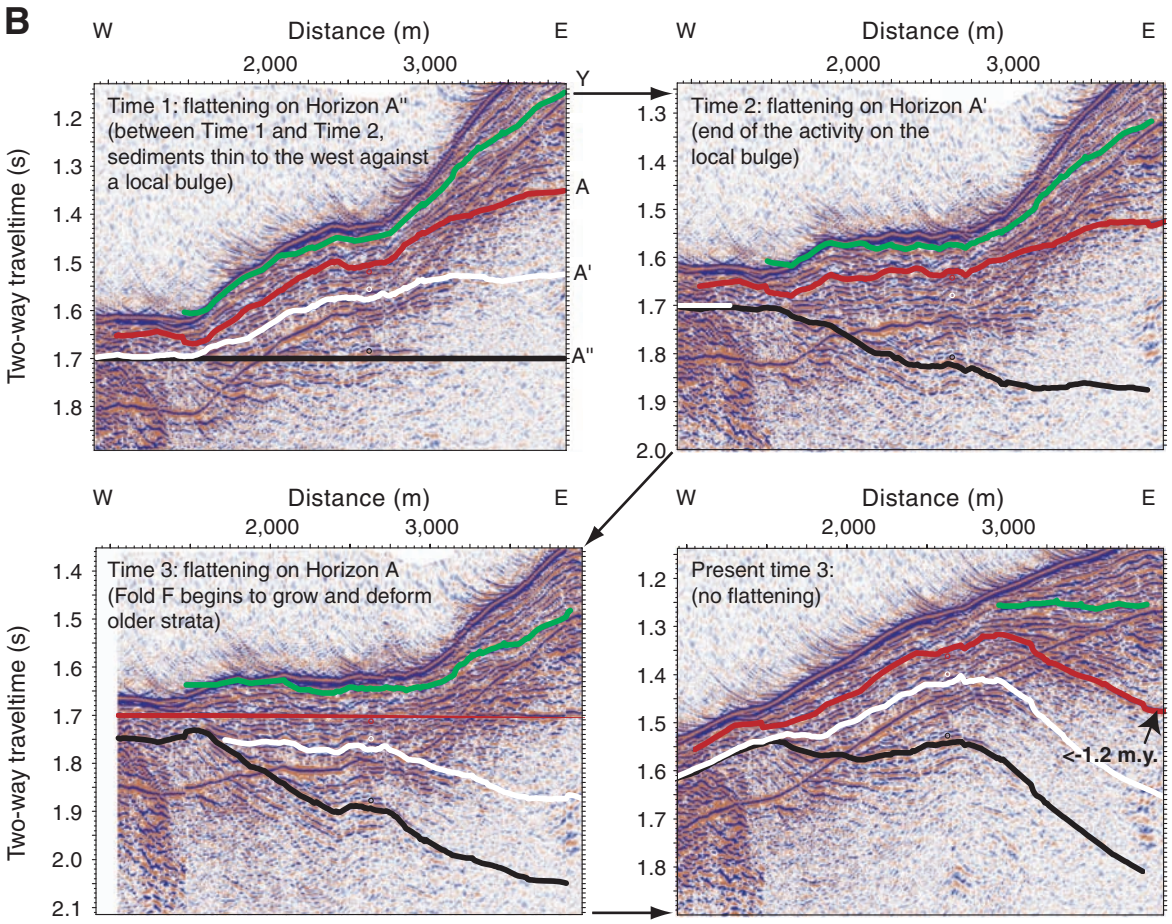

Figure F7. A. Time map to Unconformity K, which marks the boundary between seismic Units S.VI and S.VII and younger overlying strata. This map has been extended north of the 3-D survey using the 2-D profiles. It shows the circular nature of the Dome uplift and Anticlines A and B. NHR = northern Hydrate Ridge. **B.** 3-D perspective of the top of the accretionary complex. East of southern Hydrate Ridge, this surface is defined by Unconformity K; to the west, it is defined by Fold F and Fault F2 (Fig. F6A, p. 24). The northward plunge of Fold F and the southward plunge of Anticline B are apparent.

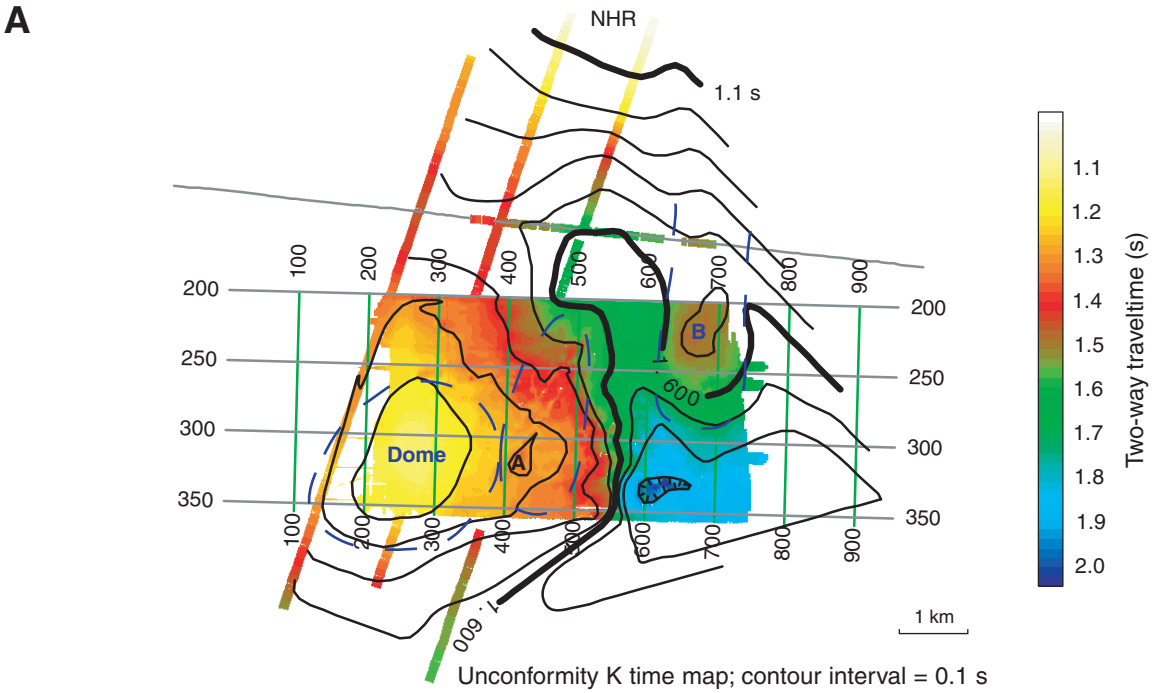

Unconformity K time map; contour interval = 0.1 s

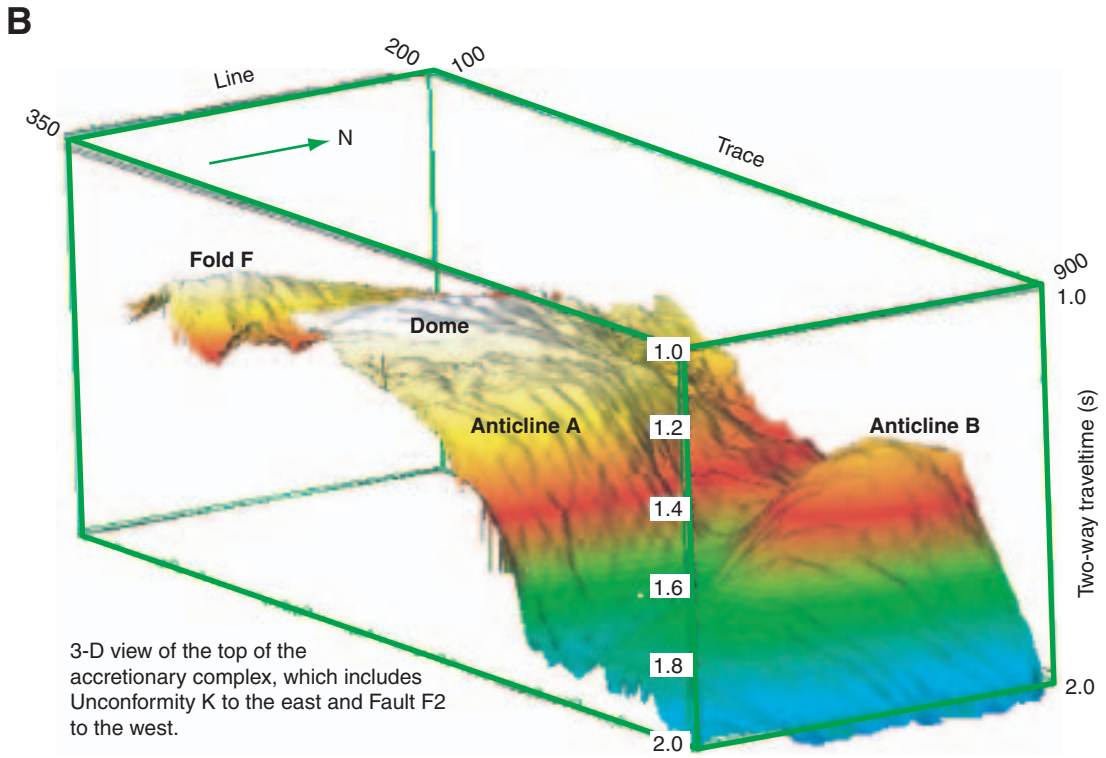

3-D view of the top of the accretionary complex, which includes Unconformity K to the east and Fault F2 to the west.

Figure F8. Isopach maps of Units (**A**) S.III, (**B**) S.II, (**C**) S.IB, and (**D**) S.IA showing the eastward migration of depocenters as the Dome underwent continuing uplift. **E.** Schematic evolution of Units S.II and S.IB based on seismic stratigraphic relationships. Evidence of continuing uplift is also seen in the stratigraphic patterns within these units, which show conformable strata downdip of offlapping strata which overlie a monocline. This reconstruction is based on the portion of 3-D Line 230 shown in Figure F3F, p. 20.

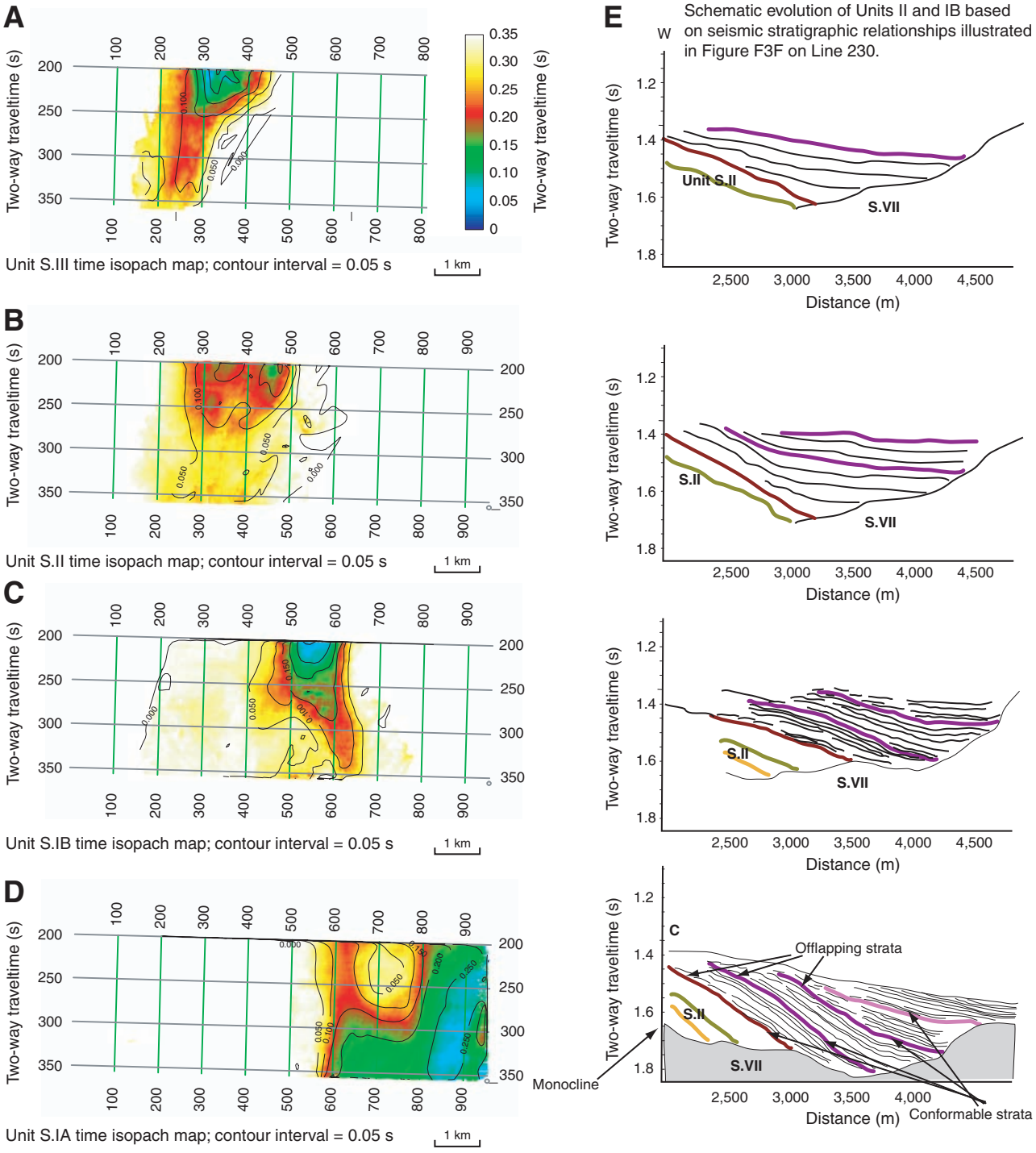

Figure F9. A. Time map to Horizon B showing a northeast-plunging anticline. This is interpreted to result from reactivated uplift of southern Hydrate Ridge (SHR). The location of the seismic section shown in part B is indicated by a thick black line. **B.** Detail of seismic data from 3-D Line 230 near Sites 1244 and 1246 showing normal faulting in Units S.II and S.IB. This faulting appears to be syndepositional and to continue to the seafloor, which shows a pattern of small northeast-trending ridges in this region (Johnson et al., 2003). These faults appear to provide pathways for migration of gas hydrate into the GHSZ, as indicated by relatively large but laterally variable gas hydrate content (Tréhu et al., 2004a) and the absence of a double BSR (Bangs et al., 2005) in this region.

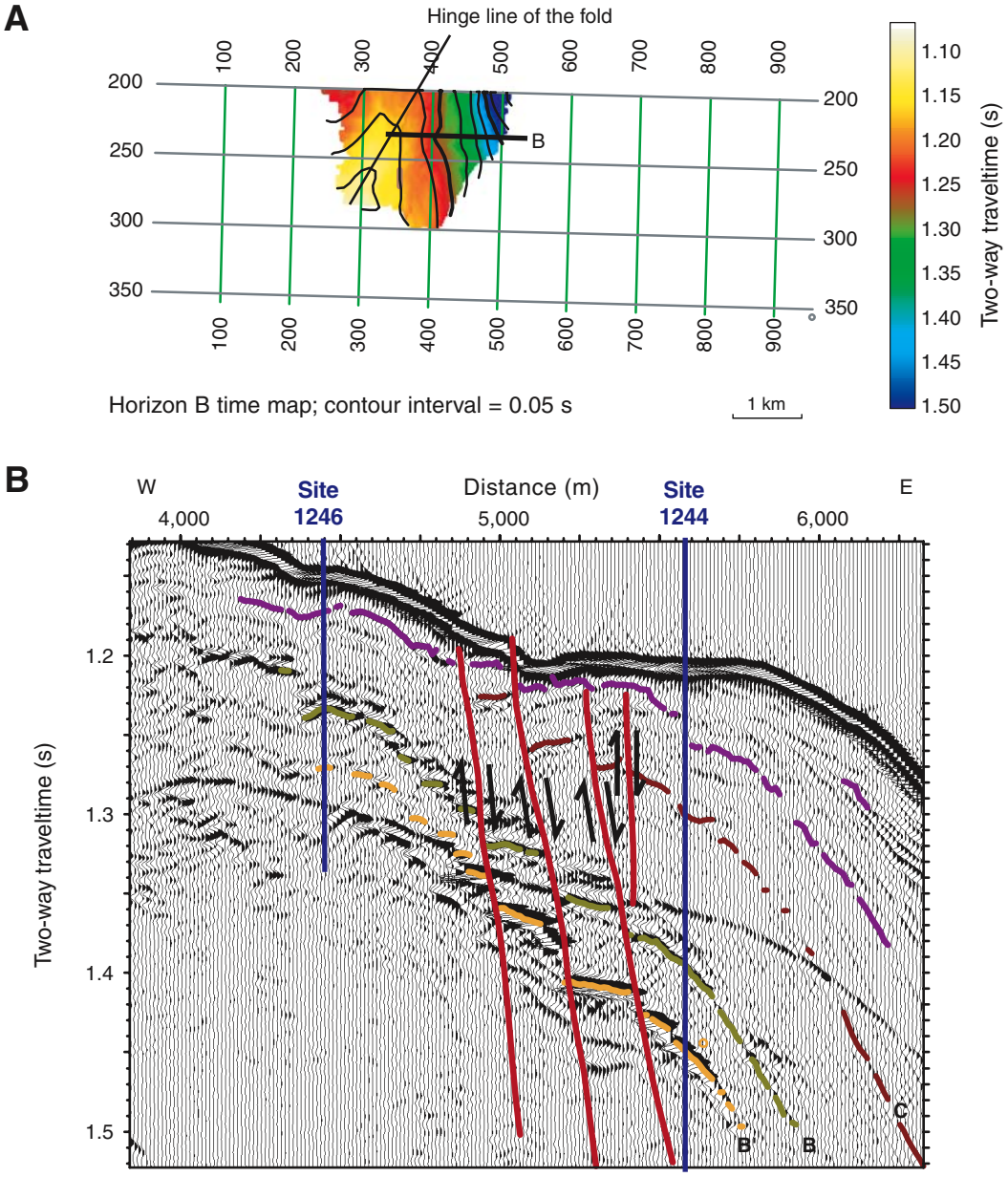

Figure F10. Sequence of reconstructed cross sections along east-west seismic Lines 230 and 300. Retrodeformation of the strata to their original geometry was achieved using rules of constant length and surface and vertical and horizontal reference pin lines (marked by a black lines and red nail). Color code and labels for structures are the same as in Figure F2, p. 18.

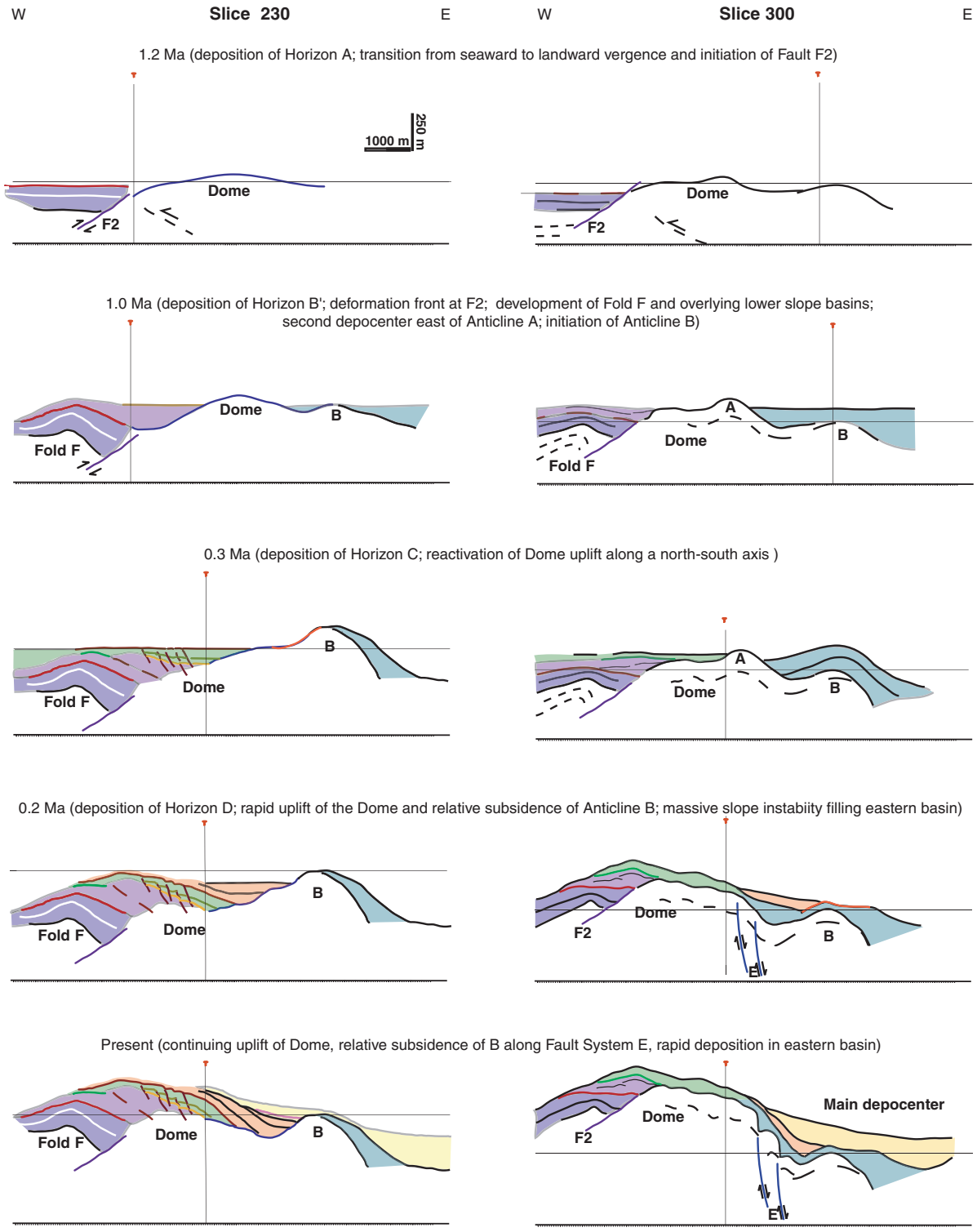

Figure F11. Map of bottom-simulating reflection (BSR) amplitude with contours showing boundaries between seismic stratigraphic units along this surface. Polarity of this reflection is everywhere negative. Orange lines indicate the intersection of seismic unit boundaries with the BSR. Labels for unit boundaries are the same as in Figure F2, p. 18.